Simulation of continuum electrical conduction and Joule heating using DEM domains

Cédric Hubert, Damien Andre, Laurent Dubar, Ivan Iordanoff, Jean-Luc Charles

DOI: 10.1002/nme.5435

Simulation of continuum electrical conduction and Joule heating using DEM domains

C. Hubert[1,*,†], D. André[2], L. Dubar[1], I. Iordanoff[3] and J.L. Charles[3]

[1]*LAMIH, UMR CNRS 8201, Université de Valenciennes et du Hainaut-Cambrésis, 59313 Valenciennes Cedex 9, France*
[2]*SPCTS, UMR CNRS 7315, European Ceramic Center, 12 Rue Atlantis, 87068 Limoges Cedex, France*
[3]*I2M-DuMAS, UMR CNRS 5295, Arts & Métiers ParisTech, 33405 Talence, France*

SUMMARY

This paper proposes an original method to simulate the electrical conduction in continuums with the Discrete Element Method (DEM). The proposed method is based on the graphs theory applied to electrical resistance network, where the resistance between two discrete elements is estimated through the notion of 'transmission surface' to assume the discrete domain as a continuous medium. In addition to the electrical conduction, the Joule heating of a DEM domain has also been developed to take full advantage of the electrical conduction. The proposed method has been implemented in the free DEM software named 'GranOO'.

The numerical results were compared against analytical approaches when applicable, or against Finite Element Method if the geometries become more complex or in case of dynamic loadings. The results are found satisfactory with errors around 3% for the electrical conduction and Joule heating of reasonably complex domains and loading cases. When it comes to more complex domains, such as electrical constriction, whilst the results remain close to those obtained with reference solutions (around 6%), they highlight the importance of taking care about the domains discretization.

Finally, the proposed method is applied to detect cracks onset on a cylindrical rod torsion test to show how to take advantage of the proposed work.

KEY WORDS: discrete element method; electrical conduction; joule heating

1. INTRODUCTION

The Discrete Element Method (DEM) was initiated in the early eighties. The article written by Cundall and Strack in 1979 [1] is considered as the first implementation of the DEM. The initial model, proposed by Cundall and Strack, studied granular media by a set of spherical pseudo-rigid bodies that interact through mechanical contacts. The aim of this method, called *particle* model, was to solve a class of problems that cannot be treated by continuous or analytic approaches such as packing problems or hourglass flows of granular media.

In the last two decades, with the spectacular improvement of computer performances, the DEM has met growing interest in the scientific community and a high number of methods based on the original DEM has been proposed in the literature. Among these methods, the *lattice* model allows us to study a continuum as a set of simple physical interactions between lattice nodes. For example, Schlangen and van Mier in [2] proposed to study the fracture of brittle solids such as concrete with a triangular lattice of mechanical beams projected on the grain structure. With such a model, the problem is that the lattice nodes are points without volume and without shape.

*Correspondence to: C. Hubert, LAMIH, UMR CNRS 8201, Université de Valenciennes et du Hainaut-Cambrésis, 59313 Valenciennes Cedex 9, France.

†E-mail: cedric.hubert@univ-valenciennes.fr

An interesting approach is to mix *lattice* and *particle* models as it was proposed by Potyondy and Cundall in [3] and Tavarez and Plesha in [4]. Mixing both approaches allows us to build a set of discrete elements where each nodes of the lattice network corresponds to the centre of a discrete element. To improve the calculation performance, the associated discrete elements are generally spherical. Therefore, the contacts between discrete elements can be treated as in classical DEM. So, complex phenomena that involve contacts in a sole body (such as closing crack lips) or between two different bodies (such as friction or sliding contact between two parts) may be tackled by mixing Lattice Element Method and DEM. However, the main difficulty of this model is to simulate quantitatively such phenomena because behaviours are generally expressed in the frame of continuum theory.

Using DEM to model electrical conduction was already achieved to study the electrical conduction of granular media such as the Branly effect of metal powders [5], the electrical conduction of powder lubricants in [6], the spark plasma sintering process [7] or the defect diagnosis by electrical measurement of ball bearing [8]. But, the mentioned studies are limited to granular media and do not deal with continuum media. This paper will introduce an original work that study the electrical conduction of continuums with DEM using arbitrary lattice networks. To validate the proposed model, the obtained results will be compared and discussed in regard of analytic solutions and classical FEM solutions.

In addition, the presented model may be coupled with thermo-mechanical DEM analyses to treat with multi-crack initiation and coalescence problems. Industrial applications such as railway transportation systems, electronics, semi-conductors or machining processes are highly concerned by the thermo-electrical-mechanical induced damages of technical parts. In such cases, where a great number of discontinuities appears, the Finite Element Method (FEM) cannot be used accurately. To demonstrate the feasibility of such an approach, the last part of this study opens on thermo-electrical-mechanical modelling. The results of thermal joule heating simulation are first presented and discussed. And then, the decreasing of the global resistivity because of brittle cracking of a rod submitted to a torsion test is presented. This last example highlights the usage of electrical measurement as non-destructive quantification of damages and shows the capability of the method to simulate such complex measurement.

2. DESCRIPTION OF THE IMPLEMENTED METHOD

2.1. Continuum Discrete Element Method domain assumption

Most of the DEM applications in electrical and thermal conduction naturally involve granular materials. The contact between two discrete elements in a DEM domain being punctual, such a method is fully appropriate for sintered materials, raw powders or ball bearings, as in the study of Bourtabache *et al.* [8] for electrical conduction, or that of Richard *et al.* [9] for thermal conduction. In these studies, the contact between particles is punctual, corresponding to infinitely small transmission surfaces.

But for some specific cases, in which the material must be assumed as continuum except its free surfaces (for example to simulate surface wear in a tribological problem, as in the study of André *et al.* [10] or that of Jerier and Molinari *et al.* [11]), the assumption of continuum discrete domain becomes relevant, and punctual contacts between discrete elements are not suitable for the propagation of an electrical or thermal field through a continuum media.

A workaround has been proposed in the field of heat transmission by Terreros *et al.* [12]. In their study, the variation of a given magnitude (the temperature in this case) for a given discrete element is the sum of the contributions of the surrounding discrete elements crossing a 'virtual' transmission surface related to discrete element i, S_i. For a simple cubic crystalline domain with equal element radii r_i, the transmission surface between two discrete elements i and j is calculated as if discrete element i was included in a cube of edge dimension $a = 2r_i$. In this specific case, the transmission surface equals $S_i = 4r_i^2$, except for elements belonging to free surfaces, edges and corners. This simple case is illustrated in Figure 1. The proposed solution for such a perfect discrete domain has been validated against the theoretical analytical solution of heat conduction [12].

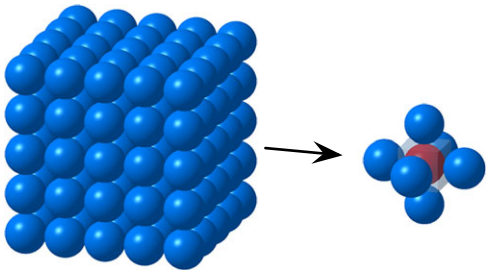

Figure 1. A simple cubic crystalline domain and an example of discrete element with six neighbours.

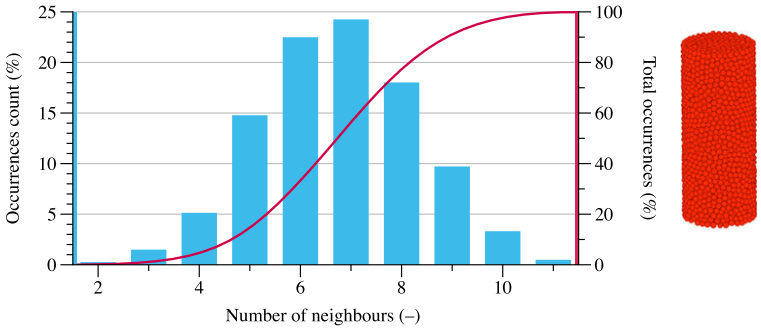

Figure 2. Neighbours count distribution for a cylindrical domain with 5000 discrete elements.

The implementation of the model presented in this paper and the validation simulations are conducted with the free DEM software 'GranOO' [13], which embeds models that enable the quantitative simulation of mechanical and thermal behaviour of continuums [14]. In the case of analyses conducted with GranOO, the discrete domains are generated thanks to a tool coming with the GranOO distribution, called 'Cooker', which fills a geometrical shape with rigid spherical elements. A uniform dispersion of 25% is applied to the element radii to avoid geometrical anisotropy [15]. The radii vary in the range of $r_i \in \bar{r}[1-0.25/2, 1+0.25/2]$, where $\bar{r}$ is the mean radius value. The estimation of the average elements radius $\bar{r}$ is based on the desired number of discrete elements using the relationship

$$\bar{r} = \left(\frac{0.63 V_g}{4/3\pi N_{DE}} \right)^{1/3}, \tag{1}$$

where V_g is the volume of the geometrical shape and N_{DE} is the desired number of discrete elements. Coefficient 0.63 approximately corresponds to the random packing density of monodisperse distribution of spheres [16].

Similarly, the average radius of the elements may be specified as an input parameter, and the final number of discrete elements becomes an output. In both cases, the generated domains are considered as correctly packed if their volume fraction is around 63%, and their cardinal number (the average number of contacts per discrete element) is around six.

Figure 2 shows the distribution of the number of neighbours for the discrete elements in a cylindrical domain with approximately 5000 elements generated with the Cooker. It shows a normal distribution which ranges between 2 and 11, with mean value $\mu = 6.7$.

In Figure 2, approximately 1200 elements have six neighbours, which corresponds to $1/4$th of the domain elements population. Thus, the use of the simple form of the transmission surface described previously $\left(S_i = 4r_i^2\right)$ would give significant errors.

Terreros *et al.* [12] proposed to estimate a transmission surface based on the number of neighbours seen by discrete element i and its radius. The cube illustrated in Figure 1 is replaced by a polyhedron with number of faces corresponding to the number of neighbours of discrete element i, and in case where such a regular polyhedron does not exist, the transmission surface is calculated from

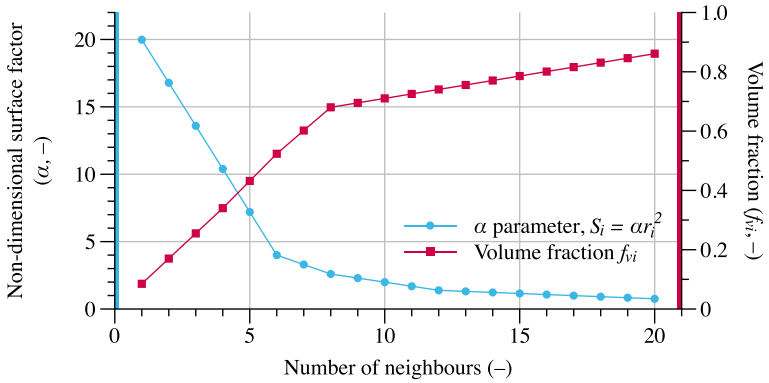

Figure 3. Transmission surface S_i and volume fraction f_{vi} as a function of the number of neighbours of element i, after [12]. [Colour figure can be viewed at wileyonlinelibrary.com]

linear interpolation. The graph in Figure 3 shows the evolution of the non-dimensional transmission surface parameter α $\left(S_i = \alpha r_i^2\right)$ according to the number of neighbours of discrete element i.

The particular condition of boundary elements must also be treated, because those elements will only have neighbours on one side, leading to an eccentricity of the neighbours packet. For instance, in the domain illustrated in Figure 1, assuming $\alpha \approx 13.6$ for a corner element would be erroneous because its three neighbours are not uniformly spread. It would actually lead to an overestimated transmission surface and thus to a decrease of the electrical resistance between this discrete element and its neighbours. This observation is also true for the edge and face elements of the simple cubic crystalline domain of Figure 1, that have four and five neighbours, respectively.

It is decided to introduce a simple factor f which value is based on the eccentricity e of the neighbours packet with respect to the observed discrete element. The eccentricity is calculated as the distance between the observed discrete element centre and the neighbours packet barycentre, normed by the observed element radius. It reads as follows:

$$e = \frac{1}{r_i} \left\| \overrightarrow{x_i} - \frac{1}{n} \sum_{j=0}^{n} \overrightarrow{x_j} \right\| \tag{2}$$

where e is the eccentricity, r_i is the radius of the observed discrete element i, $\overrightarrow{x_i}$ is its position vector, n is the number of neighbours seen by discrete element i, and $\overrightarrow{x_j}$ is the position vector of neighbour j.

In the crystalline domain illustrated in Figure 1, the eccentricity for a face element is $e = 0.4$, $e = 0.7$ for an edge element and it reaches $e = 1.2$ for a corner element. However, for well-packed domains, the number of elements with such a high value of eccentricity is small, usually below 1%. As an illustration, two distributions of the eccentricity factor e are given in Figure 4, where the graph labelled *a)* corresponds to the cylindrical domain shown in Figure 2, and the one labelled *b)* corresponds to the notched specimen with 10 000 elements used earlier as a validation case for the Joule heating implementation (Figure 10).

From the two graphs in Figure 4, it can be observed that most of the elements in both discrete domains have an eccentricity factor below $e = 0.4$ (67% for the cylindrical rod and 63% for the notched specimen), corresponding to the domains core elements. For both domains, factors higher than $e = 0.7$ represent less than 10% of the overall domains population and are mainly linked domains edges and corners, or to packing defects. As stated before, factors higher than $e = 1.2$ represent less than 1% for both domains.

Based on these remarks, and in order to keep a simple formulation of the transmission surface, the factor f will equal to one when the $e < 0.4$, and $f = 2$ when $e \geq 0.4$, corresponding to eccentricity of a face element. The final shape of the transmission surface thus reads

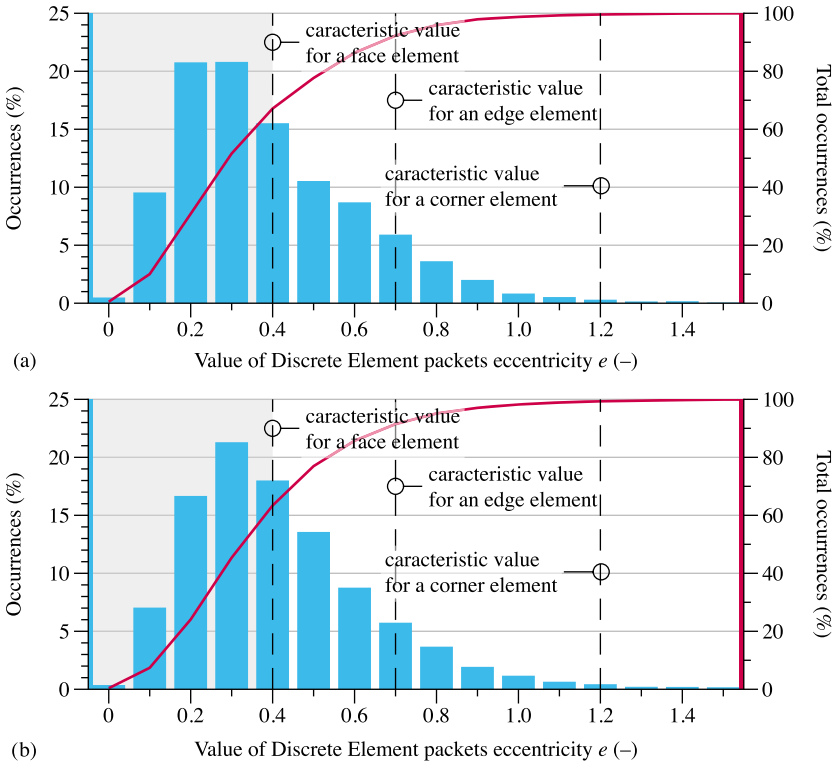

Figure 4. Eccentricity values distribution for two domains used in this paper: a) cylindrical domain with 5000 elements, b) notched specimen with 10000 elements. [Colour figure can be viewed at wileyonlinelibrary.com]

$$\begin{aligned} S_i &= \alpha r_i^2 / f, \\ \text{with} \quad f &= 1 \quad \text{if } e < 0.4, \\ \text{and} \quad f &= 2 \quad \text{if } e \geqslant 0.4. \end{aligned} \tag{3}$$

In addition to the transmission surface, the graph in Figure 3 shows the evolution of the volume fraction, also calculated by Terreros *et al.* [12], which corresponds to the volume occupied by discrete element i in the polyhedron defined by the number of neighbours of this element. As for the transmission surface, a factor $f = 2$ is applied for elements with eccentricity factor $e \geqslant 0.4$, except that it will be multiplicative instead of dividing.

In the present paper, the volume fraction will be used for the estimation of the amount of heat generated by current flow in the domain, described in Section 2.3.

2.2. Electrical conduction in a continuum Discrete Element Method domain

Because of the dynamic feature of Discrete Elements simulations, the DEM codes often use explicit schemes to compute the mechanical solutions, especially with large domains or when dynamic effects are observed. These explicit schemes require an usually small integration time step to ensure numerical stability, referred to as 'stable time step', which depends on the simulated material physical properties, namely its Young's modulus and density. In the case of a multiphysic simulation, the time step may be decreased in order to ensure the consistency of the solution linked to the fastest simulated phenomenon.

In the case of the present work, an explicit scheme is used and the propagation time of an electrical signal through a conducting medium is faster, from several orders of magnitude, than the propagation time of a mechanical front wave in the same medium. The use of the mechanical time step to solve the electrical state would lead to significant errors, and it is thus necessary to solve the electrical state apart from the mechanical integration scheme.

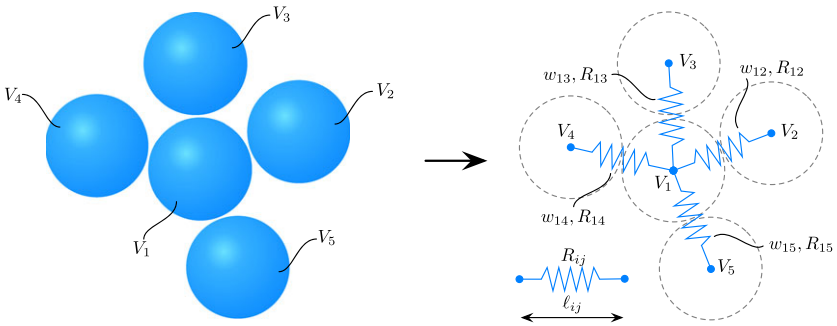

Figure 5. Illustration of an electrical circuit built from five discrete elements. [Colour figure can be viewed at wileyonlinelibrary.com]

The implemented method chosen to model the electrical conductivity is based on the graph theory applied to Ohm's law in networks, described by Strang [17]. The starting point of this method is to see the discrete domain as a large electrical resistances network, where the discrete element centres are circuit nodes, and two contacting discrete elements is a branch with resistance R_{ij}, where subscripts i and j denote the discrete elements indices. An example of such a resistance network involving five discrete elements is shown in Figure 5.

The value of the resistance formed by discrete elements i and j is calculated as the resistance of a rod with length ℓ_{ij}, cross section area (or transmission surface) S_{ij} and electrical resistivity ρ_e:

$$R_{ij} = \frac{\rho_e \ell_{ij}}{S_{ij}}, \tag{4}$$

where the electrical resistivity ρ_e has the same value as that of the raw material, that is, there is no scale effect. S_{ij} is the equivalent transmission surface between elements i and j (Equation 3), and must satisfy $S_{ij} = S_{ji}$. Because both elements may not have the same number of neighbours, the equivalent transmission surface is calculated as the geometrical average of transmission surfaces of elements i and j, and reads

$$S_{ij} = \sqrt{S_i S_j}, \tag{5}$$

where S_i and S_j are the transmission surfaces related to elements i and j, obtained from the graph in Figure 3.

The network illustrated in Figure 5 is thus composed by n nodes, corresponding to the discrete elements centres, connected to m branches, which exist when two discrete elements are in contact. These connections are recorded in matrix $\boldsymbol{A}$ called 'incidence matrix', where $\boldsymbol{A} \in \mathbb{R}^{m \times n}$. In row j of matrix $\boldsymbol{A}$, the non-zeros -1 and 1 indicate which two nodes are connected by the jth branch, the $-$ or $+$ sign being related to the node index.

In this work, the electrical conduction is considered sufficiently fast, without impedance effects nor alternating voltage source, to be assumed as steady state. The electrical potentials at nodes (or discrete elements) and currents in branches are thus calculated using the first and second Kirchhoff laws, namely:

- Kirchhoff Current Law, which states that the sum of currents entering and leaving a circuit node is zero, and
- Kirchhoff Voltage Law, which states that the directed sum of electrical potentials in a closed network is zero.

Re-writing the Kirchhoff laws and Ohm's law in matrix shape gives the following set of equations as follows:

$$\boldsymbol{A}^T w = f, \tag{6}$$

$$b - \boldsymbol{A} u = e, \tag{7}$$

$$\text{and} \quad \boldsymbol{C}^{-1} w = e. \tag{8}$$

In Equation 6, corresponding to the Kirchhoff Current Law, the incidence matrix $\boldsymbol{A}$ is transposed to access branches. This equation ensures that the sum of currents, given in vector w ($w \in \mathbb{R}^m$), in branches entering a circuit node equals the currents imposed as boundary conditions, given in vector f. The second equation of the set (corresponding to the Kirchhoff Voltage Law, Equation 7), ensures that the sum of voltages drops in vector e ($e \in \mathbb{R}^m$) in every closed loop of the circuit is zero. It depends on the voltages sources given in vector b, and on voltages at nodes listed in vector u. Finally, the voltage drops e in branches are calculated by the Ohm law, and depend on the conductance of each branch (the inverse of resistance), given by the conductance matrix $\boldsymbol{C}$, where $\boldsymbol{C} \in \mathbb{R}^{m \times m}$, and on the branches current vector w. The full system can be written in one equation, and reads

$$\boldsymbol{A}^T \boldsymbol{C} b - f = \boldsymbol{A}^T \boldsymbol{C} \boldsymbol{A} u, \tag{9}$$

or in matrix shape

$$\begin{bmatrix} \boldsymbol{C}^{-1} & \boldsymbol{A} \\ \boldsymbol{A}^{\mathrm{T}} & \boldsymbol{0} \end{bmatrix} \begin{Bmatrix} w \\ u \end{Bmatrix} = \begin{Bmatrix} b \\ f \end{Bmatrix}. \tag{10}$$

The first step to solve this equations system is to solve for u, which requires to invert matrix $\boldsymbol{K} = \boldsymbol{A}^T \boldsymbol{C} \boldsymbol{A}$. The calculation of w is then straightforward.

Inverting matrix $\boldsymbol{K}$ may be very cost effective, especially with large DEM domains. As an example, a domain with 5000 discrete elements (not considered as a large domain) has thus 5000 nodes, and approximately 16 000 branches, depending on the coordination number of the domain. Thus, the size of the square block of equations system 10 would be $(m+n)^2 = 21000^2$. Moreover, matrix $\boldsymbol{A}$ contains non-null values only when nodes connections exist, and matrix $\boldsymbol{C}$ only has the value of branches conductance in its is diagonal. The matrix system is thus sparse, and must be treated as such to save computation time and memory.

The solution adopted here for implementation in GranOO is to link the main executable with the `Eigen` C++ template library [18], which supports sparse matrices and several sparse solvers, direct or iterative. The solver chosen for this study is the Conjugate Gradient, recommended for large systems, which as been found faster than the Choleski and LU factorization implemented in `Eigen`. As an example, computation times are given in Table I for the solving of a system with 5000 discrete elements and 16 000 contacts, performed with these three solvers on an Intel Core i7-4980HQ at 2.8 GHz, with one core. Treating the system as dense has not been tested because the memory needed was to high.

2.3. Joule heating

Joule heating describes the amount of electrical energy converted to internal energy by the current flowing through a conducting medium. It is also referred to as resistive heating because of its relationship with Ohm's law. Thus, once the currents w_j in branches have been calculated (Section 2.2), the calculation of the electrical energy in each branch is straightforward and reads

$$P_{Rj} = \eta \Delta u_j w_j, \tag{11}$$

where P_{Rj} is the electrical power due to current flow in branch j, referred to as P_{Rij} in the remaining of this paper, corresponding to the electrical power released as internal heat between nodes (discrete elements) i and j. Δu_j is the potential drop in branch j and w_j is the current crossing this branch. η is a non-dimensional coefficient allowing to adjust the amount of electrical power released

Table I. Indicative computation times for a domain with 5000 discrete elements and 16 000 contacts, on an Intel Core i7-4980HQ at 2.8 GHz with one core.

Conjugate Gradient	Choleski factorization	LU factorization
24ms	33ms	114ms

as heat ($\eta \in [0,\ 1]$). If $\eta = 1$, as in the remaining of this paper, 100% of the electrical energy is assumed released as heat.

The temperature rise due to electrical power in a conductor is expressed as

$$\Delta\theta_i = \frac{P_{Rij}}{mc}\Delta t, \tag{12}$$

where m is the conductor mass, c is the conductor material specific heat capacity and Δt is the time interval during which the temperature rise is calculated. For application to the case of discrete elements simulations, the mass of each discrete element must be calculated by taking into account the volume fraction, which depends on its number of neighbours, as shown on the graph of Figure 3. The temperature rise equation for discrete element i becomes

$$\Delta\theta_i = \frac{P_{Rij}\, f_{vi}}{\rho_c c V_i}\Delta t, \tag{13}$$

where f_{vi} is the volume fraction of discrete element i, V_i is its volume and ρ_c is the material density. In a simulation conducted with GranOO, Δt corresponds to the solver stable time increment. In most applications of explicit analysis, the mechanical response will govern the stability limit. The thermal response may govern the stability limit when, for instance, mass scaling is used. The thermal and mechanical critical time steps, named respectively Δt_t and Δt_m, are calculated as follows:

$$\Delta t_t < \ell_{\min}^2/2\alpha, \tag{14}$$

$$\text{and} \qquad \Delta t_m < \sqrt{m/K}, \tag{15}$$

where $\ell_{\min}$ is the smallest distance between two discrete elements in the domain (or the shortest beam, see reference [15]), α is the material thermal diffusivity, m is the average mass of the spheres connected to the beam, and K is the beam stiffness. For the notched specimen validation model with 20 000 discrete elements (introduced in Section 3.3), the order of magnitude of the thermal and mechanical critical time steps are $\Delta t_t \lesssim 7 \times 10^{-4} s$ and $\Delta t_m \lesssim 1 \times 10^{-8} s$, and the global stable time increment is $\Delta t = \min(\Delta t_t, \Delta t_m)$.

In GranOO, equation 13 is combined, as an additional term, to the equation of temperature rise because of thermal conduction written by Terreros *et al.* ([12], Equation 7). The global temperature rise because of both electrical conduction and Joule heating reads

$$\Delta\theta_i = \sum_{j=1}^{n} \frac{(\theta_j - \theta_i) S_{ij} \lambda f_{vi}}{\ell_{ij} \rho_c c V_i}\Delta t + \frac{P_{Rij}\, f_{vi}}{\rho_c c V_i}\Delta t, \tag{16}$$

with θ_i and θ_j the temperature of discrete elements i and j, λ the material thermal conductivity and ℓ_{ij} the distance between discrete elements i and j centres (Figure 5).

3. VALIDATION OF THE IMPLEMENTED METHODS

This section aims to validate the method described in Section 2. This validation step is performed on simple DEM domains such as cylindrical rods (Section 3.1) and plates (Section 3.2) against theoretical and FEM solutions, when no simple solution exist. The effect of electric current constriction is also studied as a validation case in the same time as the Joule heating implementation validation. The material used to validate the implementations is an AISI 304L stainless steel, with data given in Table II.

All domains used in the remaining of this paper were generated using the GranOO tool 'Cooker', using the generation rules detailed earlier in Section 2.1.

Table II. Material data used for the validations cases.

Material data	Symbol	Value	Unit
Young's modulus	E	210	GPa
Poisson's ratio	ν	0.3	–
Density	ρ_c	7900	$\mathrm{kg.m^{-3}}$
Electrical resistivity	ρ_e	0.73×10^{-6}	$\mathrm{m^3kg.s^{-3}A^{-2}}$
Specific heat capacity	c	500	$\mathrm{J.kg^{-1}K^{-1}}$
Thermal conductivity	λ	15	$\mathrm{J.s^{-1}m^{-1}K^{-1}}$

3.1. Validation on uniform electrical fields

The validation of the implemented method is performed on simple cylindrical domains with radius $r_d = 1$ mm and length $\ell_d = 5$ mm, with different number of discrete elements (1000, 2000, 5000, 10 000 and 20 000) to observe the DEM calculation convergence. Moreover, each domain is generated three times to check the effect of the random filling of the geometrical container (a cylinder in this case). This validation step thus leads to 15 calculations.

The simplest way to compare the methods validity against a theoretical solution is to estimate the equivalent resistance of the domain. From the DEM side, a voltage difference is applied on the domain ends thus producing a current flow. The equivalent resistance of the DEM domain $\bar{R}_{\mathrm{DEM}}$ is calculated with Ohm's law, as the potential difference over the amount of current entering or leaving one of the domain ends. From the theoretical side, the equivalent resistance $\bar{R}_{\mathrm{th}}$ is calculated assuming a plain rod with same dimensions as the DEM domain using the common relationship

$$\bar{R}_{\mathrm{th}} = \frac{\rho_e \ell}{A}, \tag{17}$$

where ρ_e is the material electrical resistivity, ℓ is the length of the domain and A is its apparent cross section area.

Because the voltages are applied to nodes, that is, the discrete elements, the theoretical domain length ℓ must be adjusted to take into account the ends elements radius. For example, if the average radius of the elements in the domain is $\bar{r} = 106\mu$m, the effective theoretical domain length ℓ will be $\ell = \ell_d - 2\bar{r}$. On the contrary, the cross section area A actually corresponds to the domain bounding cylinder because the current density in the domain depends on the volume of the discrete element, through the transmission surface S_{ij}. An example of how are defined the values of ℓ and A is given in Figure 6.

The results are presented in Table III, which summarizes the errors compared with the theoretical solution, per domain size (with the average radius of the discrete elements) and domain generation. The results are also plotted on a graph (Figure 7) to simplify the results readability.

First, the values of errors against the theoretical solutions reported in Table III shows that the number of elements in the domain plays an important role, by decreasing the sensitivity of the solution to packing errors. It can be observed that, from a global point of view, the error stabilizes around $\sim 4\%$, for domains with discrete element count greater or equal to 5000. For the model with

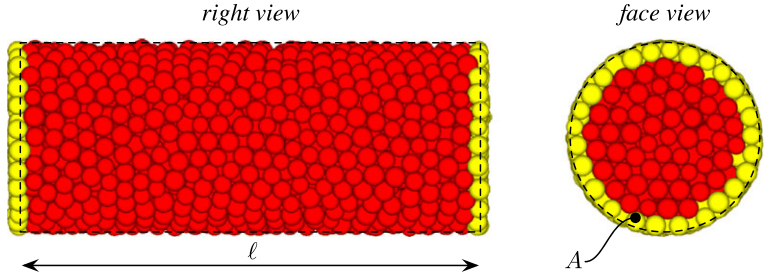

Figure 6. Determination of the domain length ℓ and cross section area A to calculate the theoretical equivalent resistance (illustration of a domain with 2000 elements).

Table III. Results of the validation based on the domains equivalent resistance, for each domain generation.

Domain size	$\bar{r}(\mu\text{m})$	Error 1 (%)	Error 2 (%)	Error 3 (%)
1000	133	6.08	10.51	9.19
2000	106	12.28	12.57	15.56
5000	78	4.11	5.80	4.04
10 000	62	4.41	3.60	3.31
20 000	49	2.60	2.92	3.04

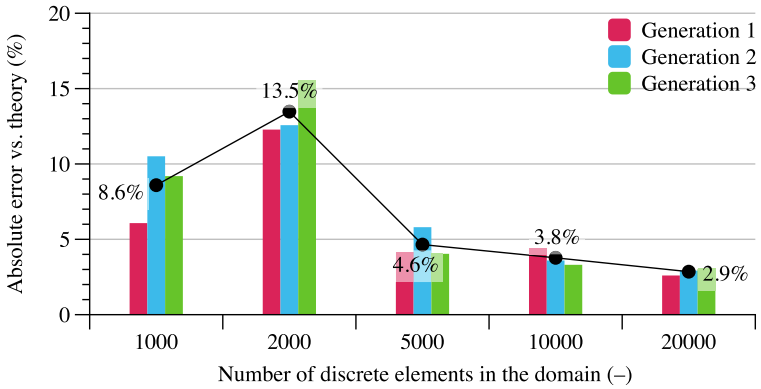

Figure 7. Validation results obtained for a uniform electrical field.

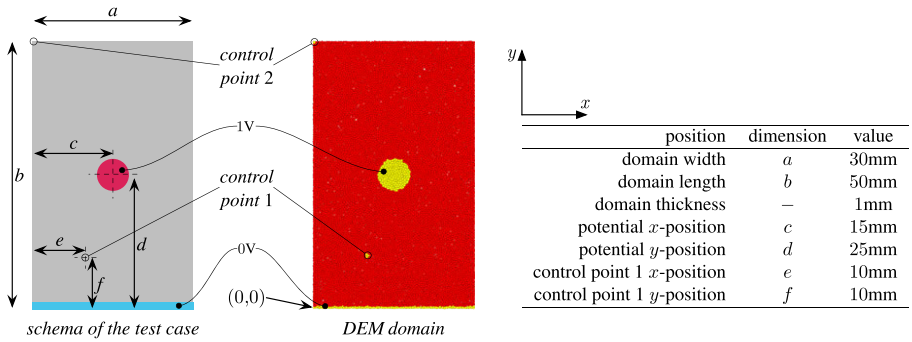

position	dimension	value
domain width	a	30mm
domain length	b	50mm
domain thickness	–	1mm
potential x-position	c	15mm
potential y-position	d	25mm
control point 1 x-position	e	10mm
control point 1 y-position	f	10mm

Figure 8. Test case configuration for the non-uniform electrical field validation.

20 000 discrete elements, the average error for the three generations equals 2.9%, which is found satisfactory. This graph also shows that a difference of about 1% may be expected between domains generations, which remains quite small. The method is thus considered as validated for uniform electrical fields.

3.2. Validation on non-uniform electrical fields

The aim of this section is to validate the developed method on domains submitted to a non-uniform electrical field. The test case chosen here is a thick plate grounded on its bottom edge, submitted to an in-depth potential of 1V, in its centre. The potential source has a diameter of 6 mm. The validation is performed by comparing the potential value at two control points with the FEM solution, using ABAQUS/Standard. The first control point is halfway between the ground and potential source, and the second one is on the top left corner. A schema of the test case configuration is given in Figure 8.

For this part of the validation, three domains are used, with 5000, 10 000 and 20 000 discrete elements, corresponding to discrete elements average radius of 408μm, 323μm and 257μm, respectively. Figure 9, shows the results in terms of error against the FEM solution at both control points, for the three tested domains.

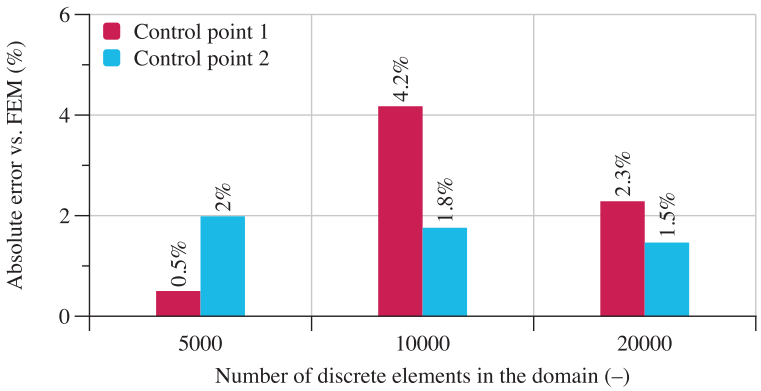

Figure 9. Results of the validation tests for a non-uniform electrical field.

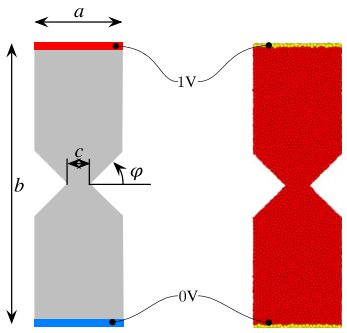

position	dimension	value
domain width	a	1.5mm
domain length	b	5mm
domain thickness	–	1mm
notch width	c	0.5mm
notch angle	φ	45°

Figure 10. Schema of the notched specimen for Joule heating validation.

As for the validation with a uniform electrical field, the results are satisfactory, with errors on both controls point lower or equal to 4.2%, and mainly around 2%. Even if no DEM domain convergence test has been performed for this part of the methods validation, the errors may change with a new domain generation due to the random feature of the filling process. But, as seen in the previous sub-section, these errors remain acceptable.

The conclusion of these first two tests is that the implemented method is reliable for both uniform and non-uniform electrical fields, the latter case being more common in the field of application of the DEM.

3.3. Validation of the thermal-electrical coupling

Joule heating is used in many applications, the closest one to the DEM being probably the sintering of metal powders, for which heating the specimens takes part in reduction of the void volume fraction. But as described by several authors [19, 20], Joule heating during sintering is believed to come from particle to particle contacts, which is not the purpose in this paper because the material is assumed as continuum. Another application lies in mechanical testing machines that involve fast heating rates. The most common specimens materials are continuous (aluminium, copper, steel, etc.) and are consistent with the continuum assumption developed in this paper.

The validation of the Joule heating implementation is performed on two kinds of DEM domains: the first one is the same rod as that used in Section 3.1, and the second one is a rectangular rod with discontinuous cross section area (a notch) to produce an electrical constriction. In the first case, the temperature in the rod will thus be homogeneous, whilst in the latter case, an increase of current density will be created in the specimen notch region. A schema of the notched specimen is given in Figure 10.

As for the previous validation cases, the DEM calculations on the cylindrical domain will be compared with the theory, because the relationship between electrical conduction and Joule heating

is straightforward in the case of a uniform electrical field (Equation 13, where the volume fraction is set to one). The simulation is performed on the domain with 5000 discrete elements, with same potential difference between the domain ends of 1V. The electrical power is considered fully released as internal heat, thus η in Equation 11 equals one. The heating process is performed during a time interval $T = 0.01$ s, and, from the DEM side, the electrical conduction will be calculated only once because the applied electrical field will not change during the simulation.

The results of the DEM simulation and the theoretical solution are given in Figure 11, in terms of temperature according to the time.

The graph of Figure 11 shows that the error between the theoretical and DEM solutions is quite small, about 1.4%. For the second test case, presented in Figure 10, the section reduction produces an electrical constriction (i.e. a local increase of current density), leading to a local temperature rise by Joule heating. The calculations are performed on four domains with 5000, 10 000, 20 000 and 40 000 discrete elements in order to highlight the effects of the increase of elements count in the notch region on the results. The corresponding discrete elements average radius are 59μm, 47μm, 37μm and 30μm, respectively. The results of these four calculations are given in Figure 12, which summarizes the errors compared with the FEM, in terms of domains equivalent resistance and final temperature in the specimens notch.

First, in terms of domains equivalent resistance, the graph of Figure 12 shows a slight decrease of the error with the increase of number of discrete elements in the domain, and thus with the number of discrete elements crossing the smallest cross section area: the error decreases in the range $[9.2\%; 6.7\%]$, whilst based on a domain slab with thickness $4\bar{r}$ ($\bar{r}$ being the average radius of discrete elements in a given domain), the number of elements in the notch increases in the range $[100; 362]$. The same observation is made for the errors in terms of temperature in the notch. The error for the domain with 5000 discrete elements is around 12%, and it decreases to 5.8% for the

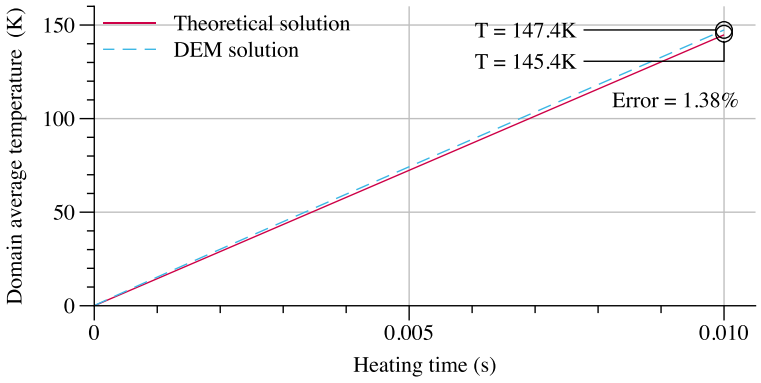

Figure 11. Results of the Joule heating of a cylindrical rod.

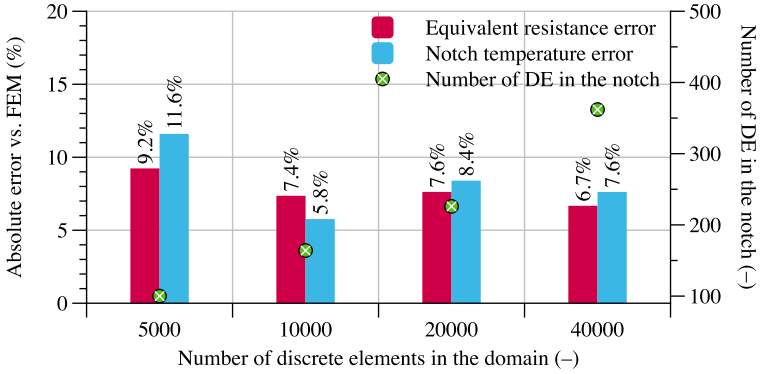

Figure 12. Results of the Joule heating of the notched domains and comparison with the FEM solutions.

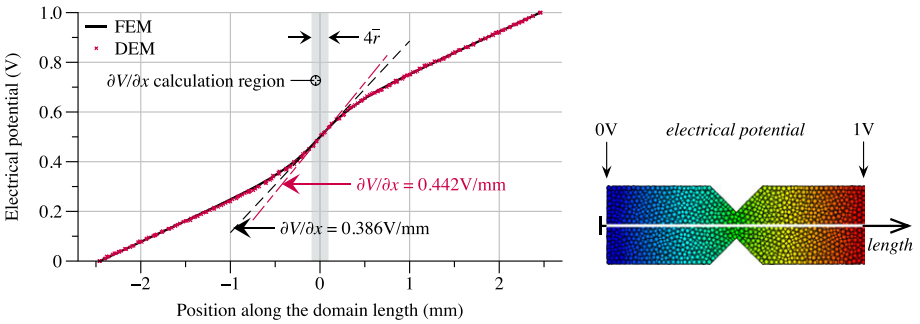

Figure 13. Evolution of the electrical potential along the domain length and illustration of Discrete Element Method result with 10 000 elements.

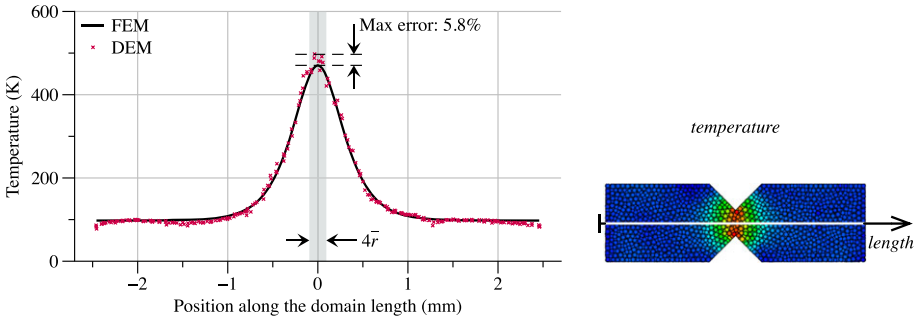

Figure 14. Evolution of the temperature along the domain length and illustration of Discrete Element Method result with 10 000 elements.

domain with 10 000 discrete elements. It remains stable around 7% for the other domains, even with more elements

This test case is very sensitive because of the notch, where few elements are responsible for the constriction resistance, which means that a local packing defect may lead to errors in the approximation of the transmission surface S_{ij} in the notch, which will be passed on subsequent calculations, such as the Joule heating. This is illustrated in Figure 13 for the domain with 10000 discrete elements.

Figure 13 shows the evolution of the electrical potential in the domain from the 0V end to the 1V end compared with that obtained with the FEM. While the global trend is perfectly represented by the DEM calculation, the gap between the two profiles increases close to the notch. It is highlighted by the slope of the electrical potential, i.e. the electrical potential gradient, defined as the potential drop per unit meter ($\partial V/\partial x$), evaluated in the region between $-/+2\bar{r}$ around the notch (greyed region on the graph in Figure 13). The potential gradient is higher for the DEM calculation (by 14.5%), which means higher local resistance for the DEM solution and eventually higher increase of temperature. The evolution of the temperature is illustrated in Figure 14, in the same way as for the electrical potential, with a comparison with the FEM solution.

As expected, and as for the electrical potential, Figure 14 shows that the maximum error on the temperature is observed in the notch region of the specimen. The global trend is correct, and the error in the notch equals 5.8% for the presented domain (with 10 000 discrete elements), which remains satisfactory. This last simple example illustrates the importance of taking care about the domains discretization, especially for non continuous electrical fields.

4. APPLICATION ON A PIN TORSION TEST

This simple application example is proposed to show how to take advantage of the electrical conduction implementation presented in this paper, with a test case which is difficult to reproduce using

the FEM, because of material failure in conjunction with electrical conduction. It is here chosen to use the equivalent resistance as an indicator of failure during a cylindrical pin torsion test. A simple cylindrical rod is submitted to a time dependent torsion angle $\dot{\theta}$ on one end, whilst the other end is clamped. The material is an ASTM 40 grey cast iron with material properties given in Table IV. The domain has a diameter $d = 1$ mm and height $h = 5$ mm, and contains 5000 discrete elements (it is the same domain as that presented in Section 3.1). Figure 15 shows the pin torsion test configuration.

The mechanical behaviour of the domain is considered as brittle-elastic and is represented by means of cohesive beams connected to discrete elements centre, as detailed in the André *et al.* study [15]. One beam exists when two discrete elements are in contact, leading in this application case to approximately 16 000 cohesive beams. The beams parameters (Young's modulus and radius) were calibrated in order to obtain a macroscopic behaviour of the domain that is consistent with the theoretical torsion solution using the procedure described in [15].

During torsion, which is considered as quasi-static (no material time dependency even if the shear strain rate $\dot{\varepsilon}$ is about 75 s^{-1}) the domain equivalent resistance is calculated as already performed

Table IV. Material data used for the pin torsion test.

Material data	Symbol	Value	Unit
Shear modulus	G	48.062	GPa
Density	ρ_c	7060	$kg.m^{-3}$
Electrical resistivity	ρ_e	0.11×10^{-6}	$m^3kg.s^{-3}A^{-2}$
Torsion (shear) yield stress	τ_y	400	MPa

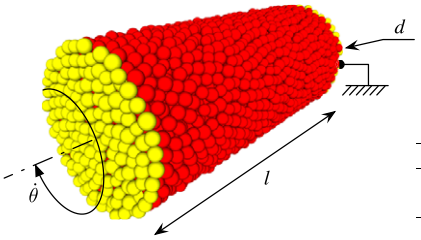

	dimension	value
domain diameter	d	1mm
domain length	l	5mm

Figure 15. Illustration of the configuration of the cylindrical pin torsion test.

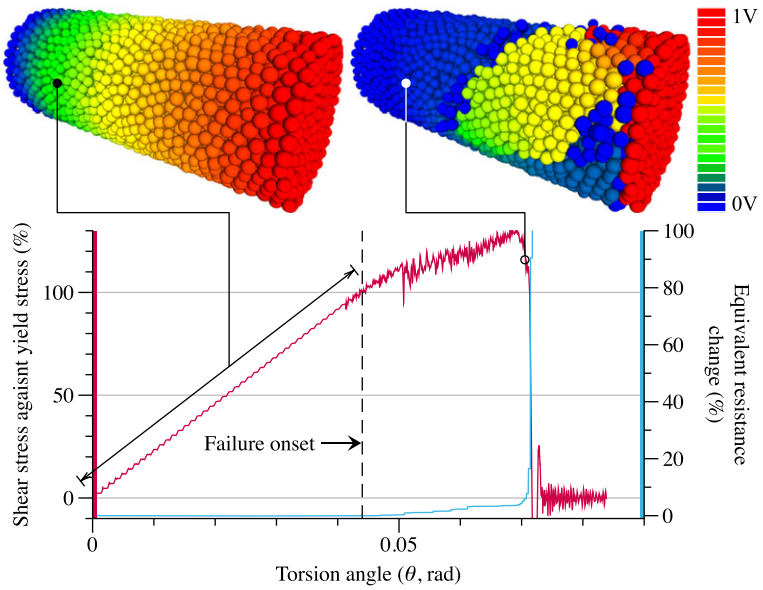

Figure 16. Results of the cylindrical pin torsion test and illustration of two major electrical states of the domain.

in the validation section: the domain is grounded in one end and the other end is submitted to an electrical potential of 1V. The evolution of the equivalent resistance is plotted on the graph in Figure 16, in addition to the percentage of stress in the domain against the shear yield stress, according to the torsion angle in radians.

In this last figure, until reaching a torsion angle $\theta \approx 0.043$ rad, the stress obviously increases linearly (not taking into account dynamic loading effects), without any significant changes in the domain equivalent resistance. The electrical potential field is continuous, as illustrated on the corresponding domain, on the left hand side of Figure 16. When the shear yield stress τ_y is reached, cohesive bonds start to break, creating cracks in the material which propagate as the torsion movement increases. These cracks produce severe electrical field discontinuities (right hand side of Figure 16), translated to an increase of the domain equivalent resistance. At the end of the simulation, for $\theta \approx 0.07$ rad, the equivalent resistance increased by more than 100%, corresponding to a cross section reduction of the same ratio (not taking into account the effects of electrical constriction). Once the specimen is completely broken, no electrical conduction can occur and the domain electrical resistance is infinite.

5. CONCLUSION

The presented work details an innovative method to study the electrical conduction with DEM. First, the assumption of continuum electrical conduction in a DEM domain is explained (Section 2.1), followed by the details of the method implemented to calculate the electrical conduction (Section 2.2) and Joule heating phenomenon (Section 2.3).

The second part of this article shows numerical application of the implemented method. The proposed test cases follow an increasing degree of complexity. It starts from simple academic configurations, where the solution can be compared with well-known analytical solutions, and it ends with complex configurations that mixes electrical and thermal problems where the solutions are compared to the FEM ones. The solutions given in terms of global electrical resistances (Section 3.1) and local potential values (Section 3.2) are in accordance with analytic and FEM solutions. In the same manner, the global temperature given by the Joule effect that involves the thermal-electrical coupling is in good accordance with analytic solution (Section 3.3). However, the validation test case that implements an electrical constriction effect is less accurate. This test case is particularly sensitive to packing defects because of the local increase of current density and the number of discrete elements in the notch region.

The last part illustrates the method with an original test case that studies the evolution of the electrical resistance during the cracking process of a grey cast iron sample due to mechanical loading (Section 4). This last example clearly shows the capability and the interest of the developed method. The coupling of mechanical phenomena, that takes into account the propagation and initiation of cracks, with thermal and electrical effects will allow to study and tackle a wide range of engineering problems that can not be treated presently with classical FEM methods.

REFERENCES

1. Cundall PA, Strack ODL. A discrete numerical model for granular assemblies. *Geotechnique* 1979; **29**:47–65.
2. Schlangen E, van Mier JGM. Experimental and numerical analysis of micromechanisms of fracture of cement-based composites. *Cement and Concrete Composites* 1992; **14**(2):105–118.
3. Potyondy DO, Cundall PA. A bonded-particle model for rock. *International Journal of Rock Mechanics and Mining Sciences* 2004; **41**(8):1329–1364.
4. Tavarez FA, Plesha ME. Discrete element method for modelling solid and particulate materials. *International Journal for Numerical Methods in Engineering* 2007; **70**:379–404.
5. Renouf M, Fillot N. Coupling electrical and mechanical effects in discrete element simulations. *International Journal for Numerical Methods in Engineering* 2008; **74**(2):238–254.
6. Zeng C, Renouf M, Berthier Y, Hamdi R. Numerical investigation on the electrical transmission ability of a shearing powder layer. *Granular Matter* 2016; **18**(2):1–7.
7. Beloni E, Santhanam PR, Dreizin EL. Electrical conductivity of a metal powder struck by a spark. *ELSTAT* 2012; **70**:157–165.
8. Bourbatache K, Guessasma M, Bellenger E, Bourny V, Fortin J. DEM ball bearing model and defect diagnosis by electrical measurement. *Mechanical Systems and Signal Processing* 2013; **41**(1–2):98–112.

9. Richard D, Iordanoff I, Renouf M, Berthier Y. Thermal study of the dry sliding contact with third body presence. *Journal of Tribology* 2008; **130**(3):031404–031404.
10. André D, Charles JL, Iordanoff I, Néauport J. The GranOO workbench, a new tool for developing discrete element simulations, and its application to tribological problems. *Advances in Engineering Software* 2014; **74**:40–48.
11. Jerier JF, Molinari JF. Normal contact between rough surfaces by the Discrete Element Method. *Tribiology International* 2012; **47**(c):1–8.
12. Terreros I, Iordanoff I, Charles JL. Simulation of continuum heat conduction using DEM domains. *Computational Materials Science* 2013; **69**:46–52.
13. The GranOO Workbench. (Available from: http://www.granoo.org/).
14. Andre D, Charles JL, Iordanoff I. *3D Discrete Element Workbench for Highly Dynamic Thermo-Mechanical Analysis: Gran00*. Wiley: London, UK, 2015.
15. André D, Iordanoff I, Charles JL, Néauport J. Discrete element method to simulate continuous material by using the cohesive beam model. *Computer Methods in Applied Mechanics and Engineering* 2012; **213–216**:113–125.
16. Finney JL. Random packings and the structure of simple liquids. I. the geometry of random close packing. *Proceedings of the Royal Society of London A: Mathematical, Physical and Engineering Sciences* 1970; **319**(1539): 479–493.
17. Strang Gilbert. *Computational Science and Engineering* (1st edn). Wellesley-Cambridge Press: Wellesley, MA, USA, 2007.
18. Eigen C++ Template Library. (Available from: http://eigen.tuxfamily.org/).
19. Carney CM, Mah TI. Current isolation in spark plasma sintering of conductive and nonconductive ceramics. *Journal of the American Ceramic Society* 2008; **91**(10):3448–3450.
20. Song X, Liu X, Zhang J. Neck formation and self-adjusting mechanism of neck growth of conducting powders in spark plasma sintering. *Journal of the American Ceramic Society* 2006; **89**(2):494–500.